ARTICLE

Direct Observation of a Carbon Filament in Water-Resistant Organic Memory

Byung-Hyun Lee,[†,‡,#] Hagyoul Bae,[†,#] Hyejeong Seong,[§,∥] Dong-Il Lee,[†] Hongkeun Park,[†,§] Young Joo Choi,[∞] Sung-Gap Im,[§,∥] Sang Ouk Kim,[∞] and Yang-Kyu Choi*[,†]

[†]Department of Electrical Engineering, [§]Department of Chemical and Biomolecular Engineering, and [∞]Department of Materials Science and Engineering, Korea Advanced Institute of Science and Technology (KAIST), 291 Daehak-ro, Yuseong-gu, Daejeon 305-701, Republic of Korea, [‡]Department of Memory Business, Samsung Electronics, San #16 Banwol-Dong, Hwasung-City, Gyeonggi-Do 445-701, Republic of Korea, and [∥]Graphene Research Center, KI for Nanocentury, KAIST, Daejeon, 305-701, Republic of Korea. [#]B.-H. Lee and H. Bae equally contributed to this work.

ABSTRACT The memory for the Internet of Things (IoT) requires versatile characteristics such as flexibility, wearability, and stability in outdoor environments. Resistive random access memory (RRAM) to harness a simple structure and organic material with good flexibility can be an attractive candidate for IoT memory. However, its solution-oriented process and unclear switching mechanism are critical problems. Here we demonstrate iCVD polymer-intercalated RRAM (i-RRAM). i-RRAM exhibits robust flexibility and versatile wearability on any substrate. Stable operation of i-RRAM, even in water, is demonstrated, which is the first experimental presentation of water-resistant organic memory without any waterproof protection package. Moreover, the direct observation of a carbon filament is also reported for the first time using transmission electron microscopy, which puts an end to the controversy surrounding the switching mechanism. Therefore, reproducibility is feasible through comprehensive modeling. Furthermore, a carbon filament is superior to a metal filament in terms of the design window and selection of the electrode material. These results suggest an alternative to solve the critical issues of organic RRAM and an optimized memory type suitable for the IoT era.

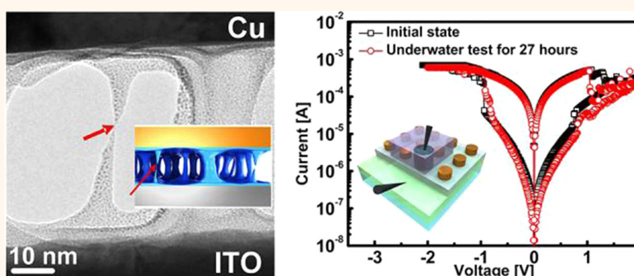

KEYWORDS: carbon filament · organic resistive memory · initiated chemical vapor deposition (iCVD) · thin nanofilm · water-resistant memory · flexible memory

The Internet of Things (IoT) represents a forthcoming technology that will change the world. IoT depends on many electronic ingredients to serve as functional blocks. One of them is high-capacity memory, which should be mounted on any substrate and which should function under any environment beyond silicon-based memory. For example, such memory should be able to be utilized to trace a distribution channel of livestock and vegetables for quarantine and disinfection and to indicate origins as well as expiration dates. Thus, it should encompass flexibility, wearability, and reliable functionality in outdoor environments in the IoT era. Although proper passivation has been used to protect devices that work outdoors, most electronic devices are still sensitive to external environmental factors. One such factor is moisture. Moisture arises from the skin of living organisms and their respiration as well as from air-bone humidity, which can cause fatal failures in memory operations. Thus, far, no stable memory device has been shown to work reliably under a fully humid condition, *i.e.*, a submerged condition, although one previous report described the operation of resistive random-access memory (RRAM) that worked with the aid of a waterproof package.[1] On the other hand, RRAM can be water-resistant due to its inherent structural simplicity and material stability compared to most types of memory highlighted thus far, including dynamic RAM (DRAM), flash-memory, phase-change RAM (PcRAM), and magnetic RAM (MRAM).

RRAM is advantageous for memory with a high packing density due to its simple structure, *i.e.*, a metal–insulator–metal (MIM) structure.[2−7] According to the material properties of the insulator, RRAM can be categorized as either organic or inorganic RRAM.[4−6] In particular, the use of a polymer, a versatile organic material with good mechanical strength, has recently contributed

* Address correspondence to ykchoi@ee.kaist.ac.kr.

Received for review April 13, 2015 and accepted June 9, 2015.

Published online June 09, 2015
10.1021/acsnano.5b02199

© 2015 American Chemical Society

to the development of flexible and wearable memory due to good flexibility, low cost, and simple fabrication such as direct printability. In this respect, organic RRAM can be an attractive candidate as memory for use in the IoT. Thus far, most reported organic RRAM has relied on solution-process-oriented polymerization. However, it has fatal weaknesses: the limited available substrate and side effects arising from the solvent.[8,9] Moreover, the unclear switching mechanism of organic RRAM is a technical obstacle that prevents reproducibility and comprehensive modeling,[4−6] which are essential in the design of device parameters. Although various possible switching mechanisms such as charge transfer,[10] space charge and traps,[11] and filamentary conduction (FC)[12,13] were reported, they still remain subjects of debate because direct evidence is very rare. Thus, the absence of a clear switching mechanism and the limitation of the solution process are critical problems that should be solved prior to the implementation of RRAM in the IoT.

In this study, we demonstrate i-RRAM, a type of RRAM based on a new organic material, *i.e.*, iCVD-polymer-intercalated RRAM. The polymer applied in this work was deposited by use of an initiated chemical vapor deposition (iCVD) process, which is an all-dry vapor-phase technique (Supporting Information). The polymeric layer created by the iCVD process has high conformability (step coverage) and good purity without solvent and another impurity, and it can strongly adhere to any substrate by surface-growing characteristics.[8,9,14] Due to the high chemical purity and nanoscale thickness controllability of the iCVD process, the iCVD-grown polymer film can be used as an insulating layer for versatile electronic devices.[15] Here, we chose poly(ethylene glycol dimethacrylate) (pEGDMA), with a highly cross-linked structure, which confirms that the polymer has proper band structure as an insulator (Supporting Information).[16] The i-RRAM showed robust flexibility and stable operation, even under water, which originates from the high water stability of the pEGDMA layer. In addition, direct observation of a carbon filament by means of cross-sectional transmission electron microscopy (TEM) is reported for the first time, in which the switching operation of the i-RRAM is attributed to the resistive switching layer (RSL), *i.e.*, pEGDMA, not an effect of the electrode. Additionally, the switching mechanism in the i-RRAM is supported by an analysis of the current (I)−voltage (V) characteristics, by conductive atomic force microscopy (C-AFM) data, and by energy-dispersive X-ray spectroscopy (EDS) data. Two types of filamentary conduction, with a metal filament and with a carbon filament, were reported in the organic RRAM.[3,4] There have been a few direct observations of a metal filament.[17−19] However, there has been no direct observation of a carbon filament, although a conceptual hypothesis was proposed by Pender *et al.* in 1975.[20] Moreover, it should be noted that the switching mechanism governed by the carbon filament is preferred to that by the metal filament because the former is not affected by the selection of the metal electrode. This aspect is desirable to provide more degrees of freedom when designing versatile RRAM fitted for the IoT.

RESULTS AND DISCUSSION

The memory operation and a schematic of the i-RRAM, demonstrating its simplicity, are illustrated in Figure 1a. The i-RRAM exhibited a low operation voltage near ±1 V for effective power consumption and an acceptable memory window above 10^2, which is the ratio of high resistance in an off-state to low resistance in an on-state. Moreover, it does not require any pre-electroforming process, which is one disadvantage of other types of resistive memory. Also, Figure 1b shows that the i-RRAM can operate as a nonpolar resistive memory, which has no dependency on bias polarity for SET and RESET operation. This nonpolar switching mode allows for a high degree of freedom when designing versatile resistive memory. The cross-sectional TEM image shown in the inset of Figure 1b shows a 50 nm thick RSL deposited by iCVD that is uniformly formed between the top electrode (TE) and bottom electrode (BE). As mentioned above, iCVD is the versatile process that boasts a superior coating capability of the polymer layer on any substrate due to the room-temperature-based process and all-dry vapor-phase technique (Supporting Information). In order to analyze the switching mechanism, Figure 1a was replotted as a log−log scale in Figure 1c. A high resistance state (HRS) before the SET process is categorized by each operational mechanism based on the trap-controlled space-charge-limited conduction (SCLC)[18,21] region: an ohmic region, a Child's law region, and a steep slope region. In contrast, the I−V relationship in a low resistance state (LRS) after the SET process shows only an ohmic property, which corresponds to filamentary conduction induced by the formation of a conductive channel linking TE and BE.[18,22] The distinctive feature of the filamentary conduction is the formation of a localized physical conduction path. In this respect, C-AFM is a direct method that can be used to confirm filamentary conduction.[17,23] Figure 1d shows the result of C-AFM for analyzing the distribution of the current in the HRS and the LRS. The distribution of the negligible and uniform current in the HRS is confirmed over the entire scanned area. In contrast to the HRS, the result of the LRS shows a nonuniformly distributed current with a very large peak value, which signifies the random formation of the filament with varied resistance.

Two types of filamentary conduction have been suggested thus far in organic RRAM. One is metal filamentary conduction,[24] which has been steadily

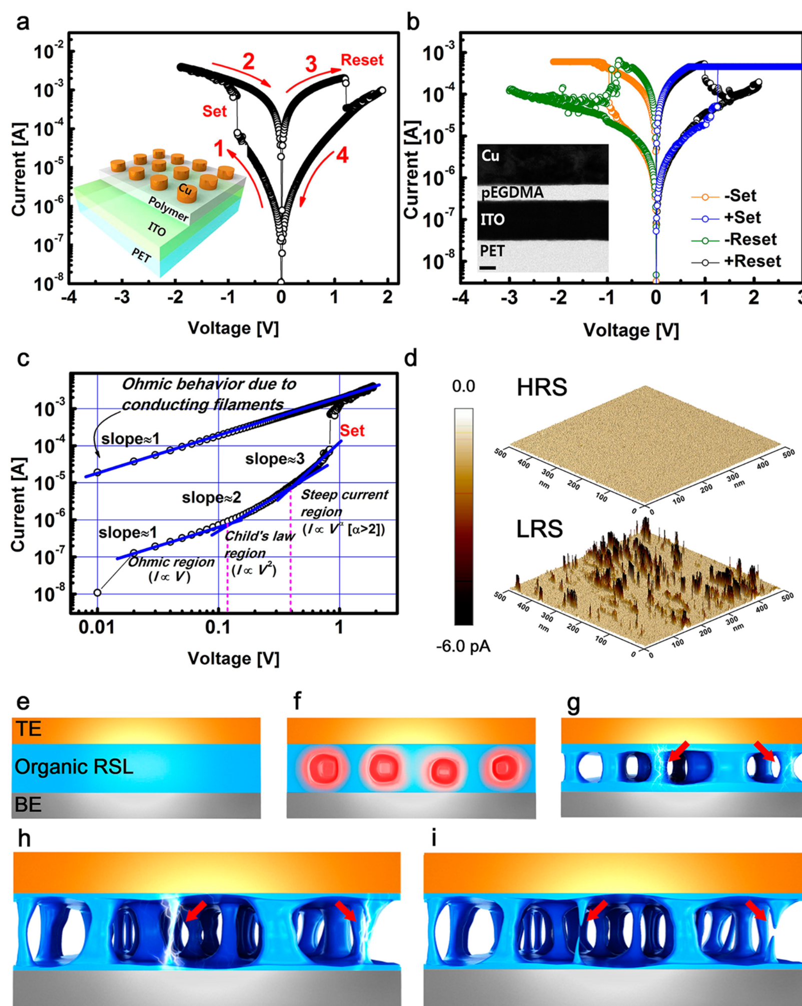

Figure 1. Memory operation and switching mechanism. (a) Bistable memory operation with the bipolar switching mode. The arrow signifies the sweep of the applied voltage. While the 1, 2 process leads to the on-state of the memory via the SET operation, the 3, 4 process gives rise to the off-state *via* the RESET operation. The inset image shows a schematic of the fabricated i-RRAM. (b) Nonpolar switching property of i-RRAM. i-RRAM exhibits a memory function regardless of the bias polarity. Unipolar-switching-based memory operation symmetrically occurs at both positive and negative bias regions. The inset image shows a cross-section TEM image. (c) $I-V$ curve with log−log scale. The conduction mechanism of the i-RRAM from the HRS to the LRS is analyzed, which is identical under the reverse condition, *i.e.*, the LRS to the HRS. (d) Result of C-AFM to analyze the filamentary conduction. (e) to (i) show a schematic that elucidates the carbon filamentary conduction mechanism. (e) Pristine state. (f) Beginning of the pyrolysis of the polymer due to Joule heating induced by the applied bias. (g) Formation of a conductive carbon-rich region surrounding the intensified pyrolysis of the polymer. (h) Formation of conductive carbon filament bridging of TE and BE, in which the arrow indicates the formed carbon filament. (i) Rupture of the carbon filament due to the added thermal driving.

researched based on acceptable experimental results.[17,19] However, metal filamentary conduction causes the following issues: a limitedly available metal electrode,[24] the need for a pre-electroforming process,[25] and damage of the metal electrode.[26] The other is carbon filamentary conduction,[20,22,27,28] whose research progress is still in an early stage, without reliable results. Here, the i-RRAM exhibited a distinctive switching operation that does not depend on the bias polarity and a pre-electroforming process. Moreover, all possible resistive switching modes regardless of bias polarity, electrode metal, and the fabrication process of the electrode are provided in the Supporting Information. That is, the switching property is governed by the inherent characteristic of the RSL without the aid of a metal, which can resolve the fundamental limitations of the metal filament. These results indicate that i-RRAM is controlled only by carbon filamentary conduction regardless of the metal used.

Sequential schematics of the carbon filamentary conduction are well illustrated in Figure 1e to i according to the results of this study and previous research results.[18,27] When bias is applied to the initial device in Figure 1e, Joule heating triggers a local breakdown at the weakest point inside the polymer and starts to make voids as shown in Figure 1f. An increase of the applied bias accelerates the local breakdown, *i.e.*, pyrolysis, and then it concurrently makes the localized region surrounded by voids become more conductive. This state is illustrated in Figure 1g. The pyrolysis of the

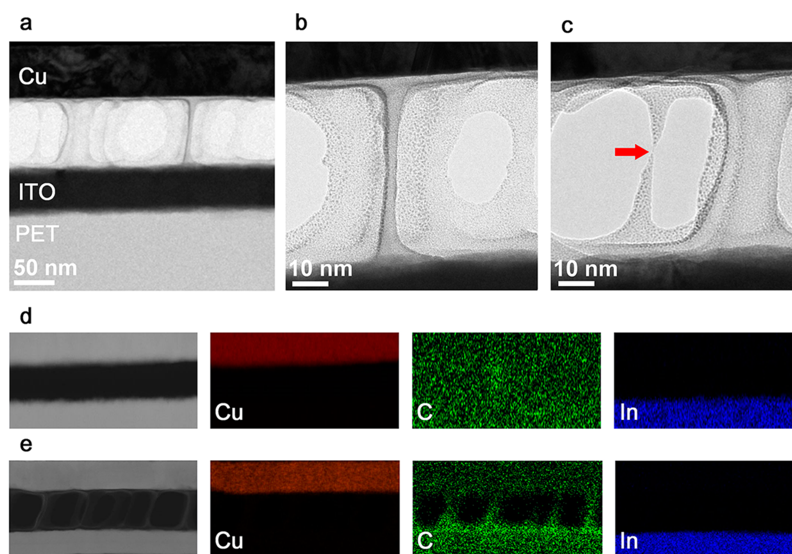

Figure 2. TEM and EDS mapping image of the carbon filament. (a) Cross-section TEM image after repetitive memory operations. (b) TEM image of the carbon filament formed for LRS. According to previous research,[20] a breakdown region such as a void is formed by the pyrolysis of the polymer, in which thermal driving due to Joule heating leads to pyrolysis from the weakest point and simultaneously the formation of a conductive carbon-rich region surrounding the breakdown region. (c) TEM image of the carbon filament ruptured for the HRS, in which the arrow indicates the ruptured point contributing to a return to an HRS. (d) EDS mapping image of the pristine state before memory operation. (e) EDS mapping image of the state after repetitive memory operations. Only the carbon in the RSL showed a variation, as detected before and after the memory operation, which signifies that the memory operation is due to the variation of the RSL, *i.e.*, the pEGDMA itself and not the TE or the BE.

polymer due to the Joule heating can change the conductivity of the initial polymer.[18,29,30] As the bias approaches the SET voltage, Figure 1h shows the formation of an ultranarrow and highly conductive carbon filament that connects the TE and BE. Thereafter, this results in a LRS, *i.e.*, an on-state. The added thermal energy causes a rupture in the carbon filament at the weakest point, which is made at the middle of the filament preferentially, as shown in Figure 1i.[3,4] Finally, the device returns to an HRS, *i.e.*, an off-state.

Clear evidence of the carbon filament is shown in Figure 2 for the first time through the use of TEM analysis after iterative memory operations, and Figure 2b and c clearly show the formation and rupture of the carbon filament due to pyrolysis. The randomly distributed carbon filaments in Figure 2a are attributed to the pyrolysis of the polymer owing to the Joule heating.[20] Thus, an LRS is made. Figure 2c displays an image of a ruptured filament reflecting a schematic reported previously,[3,4] which contributes to returning the device to an HRS. Figure 2d and e present EDS mapping images of the i-RRAM before and after the memory operation. The EDS result proves that nothing changed in both the TE and BE; that is, there was no interaction with the RSL. In contrast, the carbon image in Figure 2e, which is similar to the filament linking between the TE and the BE, is distinct from that in Figure 2d. It is noteworthy that only carbon (C) is detected in the resistive polymer layer, and no other conductive materials such as Cu from the TE and In, Sn, and O from the BE are found, even after iterative memory operations. Consequently, the result of Figure 2 validates the theory of carbon filamentary conduction and proves the obvious switching mechanism in the i-RRAM.

As shown in Figure 3a, the i-RRAM exhibits a prolonged retention time that exceeds 10^6 s and an acceptable memory window (the current ratio of the on-state to the off-state) larger than 10^2 after cyclic switching hundreds of times. This result demonstrates the feasibility as a reliable nonvolatile organic memory, supporting the stability of a carbon filament in the organic layer, *i.e.*, pEGDMA. Figure 3b shows the fluctuation of the operational voltage below 2 V, which supports operational stability at a low voltage in the i-RRAM. Figure 3c and d present the high flexibility of the i-RRAM. The i-RRAM showed stable memory operations up to a bending radius of 4 mm, and the reliability was verified by a robust bending endurance of more than 10^3 cycles. Also, the i-RRAM boasts potential as an easily attachable memory suitable for the IoT era, as shown in Figure 3e and f. The i-RRAM can serve as flexible memory on “things” of the IoT with a significantly curved structure such as a laser pointer and a finger. Furthermore, the result shown in Figure 3f opens the possibility for epidermal electronics over wearable electronics considering that the iCVD layer can be used on any substrate due to the inherent room-temperature process.

Water causes a fatal failure even to the device protected by proper passivation. Therefore, a water-resistant characteristic is essential for the memory to be used in the IoT era. The water-resistant feature of

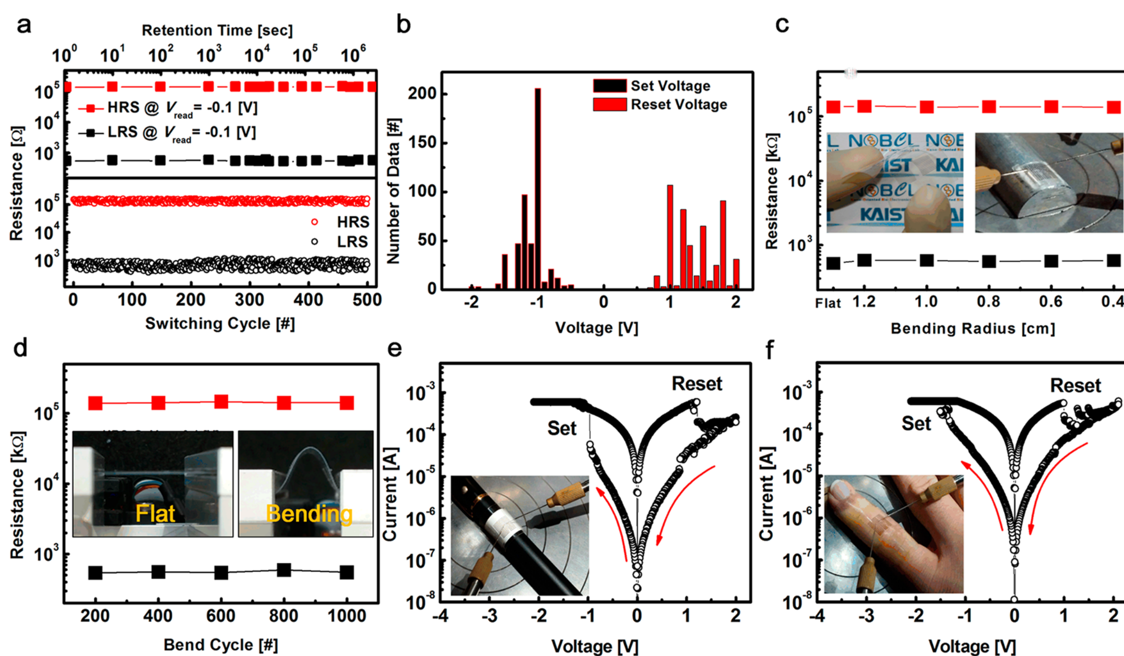

Figure 3. Memory effect, flexibility, and easy attachability of i-RRAM. (a) Variation of the HRS and LRS as a function of the retention time and the switching cycle. Here one switching cycle includes one full sweep for memory operation, *i.e.*, SET for LRS and RESET for HRS. (b) Voltage distribution for the SET and RESET operation. The data were extracted during the 500th switching cycle. (c) Variation of the HRS and LRS as a function of the bending radius. (d) Variation of HRS and LRS as a function of the bending cycle. A custom-made bending machine was used to evaluate the bending endurance at a radius of 0.4 cm. (e) *I*−*V* characteristics for memory operation on a laser pointer. (f) *I*−*V* characteristics for memory operation on a finger. The i-RRAM, with remarkable flexibility, is easily attachable onto various curved structures. It should be noted that the use of any substrate due to the room-temperature process of the iCVD can permit a wide variety of applications such as paper and epidermal electronics.

the i-RRAM is demonstrated in Figure 4. Figure 4a shows the *I*−*V* characteristic before and after submergence as well as the on- and off-state current for various submerged times. These experiments were conducted outside of the water after drying the device. The i-RRAM exhibits an invariable *I*−*V* characteristic and on- and off-state current even after submergence for 27 h, thereby resulting in a stable memory window, as shown in Figure 4b. In an extension of these experiments, the memory operation was further evaluated in water. However, an underwater experiment requires a prerequisite condition to prevent an electrical short between the TE and the BE, which was optimized *via* the setup shown in the inset of Figure 4d. The measurement details are included in the Supporting Information. As a consequence, the experimental result in water was also similar to that out of the water (Figure 4c), which demonstrates that the i-RRAM is robust to water.

In order to verify the water-resistant characteristic of i-RRAM, the stability of the pEGDMA film in water was evaluated *via* analysis in the bulk and on a surface. Figure 5a shows the analysis result of X-ray photoelectron microscopy (XPS) of as-deposited pEGDMA and pEGDMA exposed to water for 27 h. The invariable chemical structure and the atomic portion between the two states demonstrates that the backbone groups in the pEGDMA thin film were well preserved after long-term exposure to water. In addition, Fourier transform infrared spectroscopy (FT-IR) was measured to observe the changes in the chemical bonds in the pEGDMA thin film before and after exposure to water, which is shown in Figure 5b. No noticeable changes were observed in the pEGDMA thin film even after exposure to water for 27 h, which supports the high chemical stability of the pEGDMA thin film. The changes of the thickness and film morphology between the pEGDMA films under the two states were monitored *via* AFM. As shown in Figure 5c, negligible changes in both the thickness and roughness were observed, indicating that no swelling or delamination was occurring in the pEGDMA thin film. Finally, changes in the surface energy of the pEGDMA before and after water exposure were also examined. To measure the surface energy, the contact angle of two liquids, water and diiodomethane (DIM), were evaluated in advance. As a result, the calculated surface energy showed no notable variation, as shown in Figure 5d (Supporting Information). These results indicate that the surface and bulk property of the pEGDMA were highly stable even after long-term exposure in water, which supports the water-resistant characteristics of the i-RRAM.

CONCLUSIONS

In summary, we demonstrated flexible, wearable, and water-resistant organic memory with an obvious

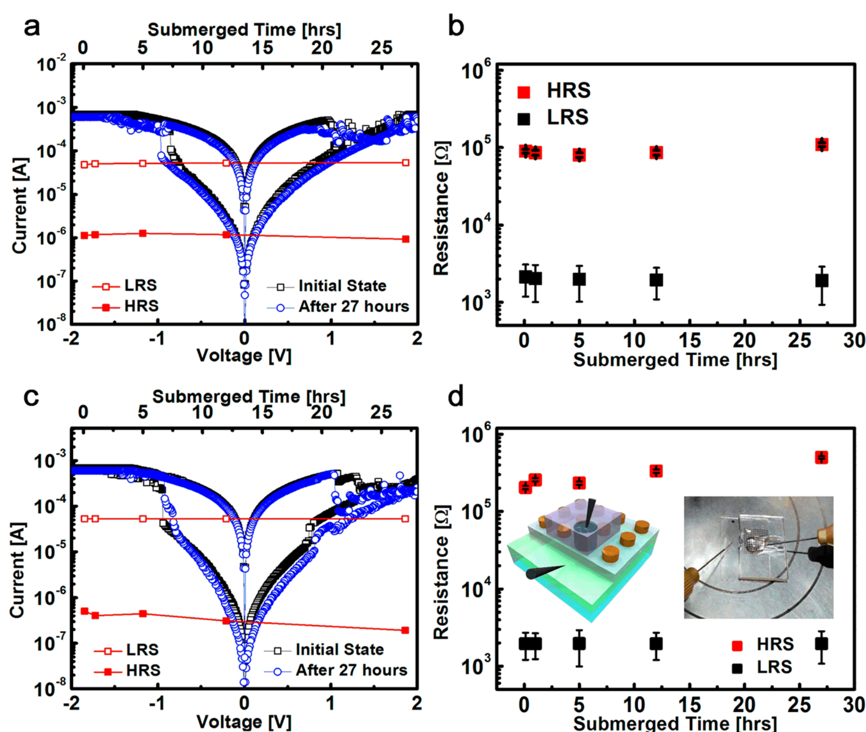

Figure 4. Water-resistant i-RRAM. (a) *I*−*V* characteristic and the LRS and HRS current, *i.e.*, the on- and off-state current as a function of the submerged time. The black- and blue-colored curves exhibit the *I*−*V* characteristic before and after a submerged time of 27 h. The red-colored curves present the on- and off-state current as a function of the submerged time, in which the current was measured at a reading voltage of −0.1 V. The electrical data were obtained out of the water after drying the device. (b) Variation of the HRS and LRS as a function of the submerged time. That is, it shows a stable memory window even after a submerged time of 27 h. (c) *I*−*V* characteristic and on- and off-state current as a function of the submerged time. Although (c) is similar to (a), (c) is the result evaluated in water, not out of the water. (d) Variation of the HRS and LRS as a function of the submerged time. The measurement setup to prevent an electrical short between the TE and BE due to water is shown as an inset image by a schematic and an actual image, respectively. The i-RRAM showed stable memory operation even after 27 h in water, which demonstrates the strong chemical stability of the iCVD-based polymer against water.

switching mechanism: the formation and rupture of a carbon filament. The employment of iCVD for organic RRAM overcame the fundamental limitations of the solution process. Note that the iCVD, applicable to any substrate, was useful for flexible and wearable electronics. Also, the iCVD-based polymer, with high purity and strong adhesion to any substrate, showed robust immunity to chemical and mechanical stimuli, as demonstrated through a bending endurance test and strong durability against water. The i-RRAM, with robust flexibility and good water resistance, can contribute to the design of versatile memory chips in the IoT era. In order to resolve the controversy surrounding the switching mechanisms of organic RRAM, clear evidence of the carbon filament using TEM was here reported for the first time. Also the carbon filamentary conduction was supported by EDS and C-AMF analyses and by the previously reported hypotheses. Additionally, it was electrically verified by the unique memory operation with various features such as the lack of an electroforming process, no dependency on a metal electrode, and nonpolar switching. It is inferred that the clear switching mechanism can allow comprehensive modeling, which can then enhance performance with high reproducibility. Consequently, the results of this study represent a green light for finding an optimal memory devoted to IoT applications as well as a solution to the critical problems associated with organic RRAM.

METHODS

As shown in Figure 1a, the i-RRAM has a simple capacitor-like MIM structure that consists of an organic restive switching layer sandwiched between a top electrode and a bottom electrode. Therefore, the fabrication method is also very simple. ITO-coated polyethylene terephthalate (PET) with thicknesses of 80 nm and 125 μm is used as the BE and the flexible substrate, respectively. Subsequently, the iCVD-based polymer named pEGDMA is introduced as an RSL for the i-RRAM. A polymerization process of the pEGDMA followed, as noted in the Supporting Information. The thickness of the deposited polymer films was monitored *in situ* by a He−Ne laser interferometer system. After the polymerization of the RSL using the iCVD, Cu with a thickness of 100 nm was deposited by a thermal evaporation process to form the TE, with a deposition rate of 0.6 Å/s. The patterning of the TE was simultaneously fulfilled by a custom-made shadow mask with a diameter of 250 μm during the deposition of the Cu. All electrical measurements were carried out in an ambient air environment without any device encapsulation. The electrical

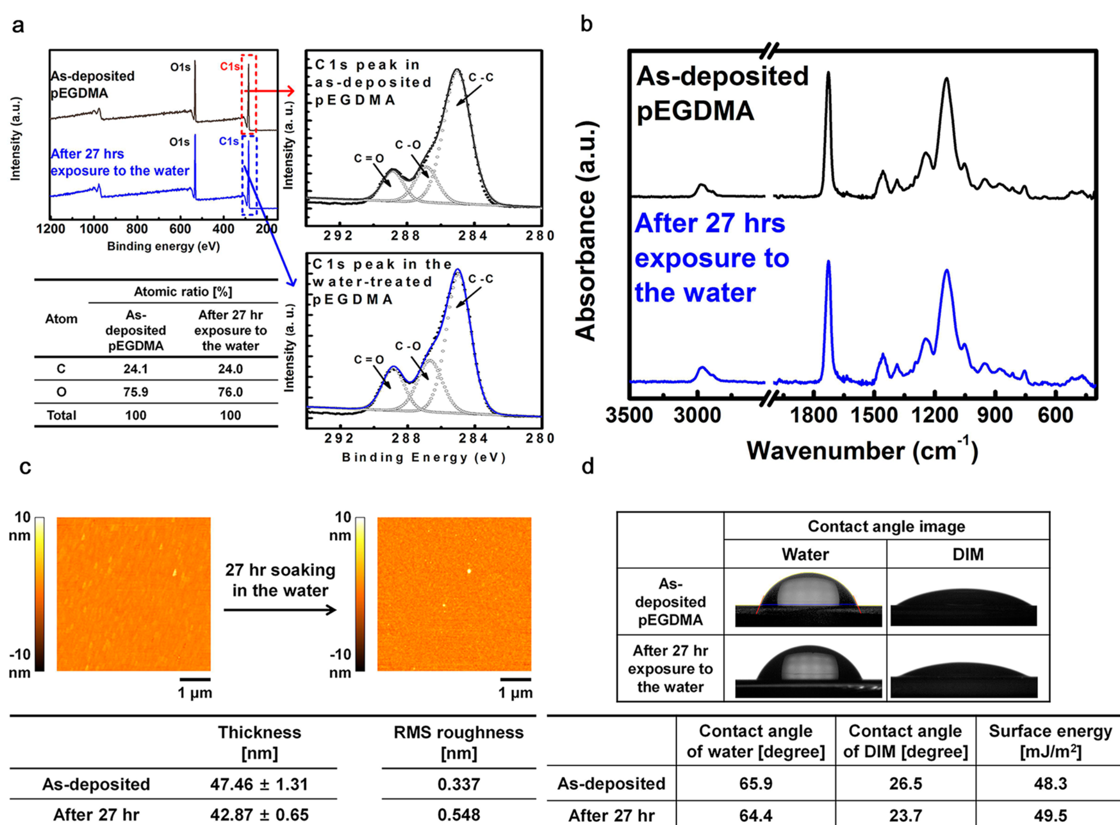

Atom	Atomic ratio [%] As-deposited pEGDMA	After 27 hr exposure to the water
C	24.1	24.0
O	75.9	76.0
Total	100	100

	Thickness [nm]	RMS roughness [nm]
As-deposited	47.46 ± 1.31	0.337
After 27 hr	42.87 ± 0.65	0.548

	Contact angle of water [degree]	Contact angle of DIM [degree]	Surface energy [mJ/m²]
As-deposited	65.9	26.5	48.3
After 27 hr	64.4	23.7	49.5

Figure 5. Analysis of water-resistant characteristic. (a) Stability of the pEGDMA thin film in water. XPS survey spectra and high-resolution scans of as-deposited pEGDMA and pEGDMA exposed to water for 27 h were measured. The invariable chemical structure and the atomic portion between the two states verify the high stability. (b) FT-IR spectra of as-deposited pEGDMA and pEGDMA exposed to water, respectively. There was no change between the two samples. (c) AFM images of as-deposited pEGDMA and pEGDMA exposed to water, respectively. The table below indicates the changes in the thickness and RMS roughness of the pEGDMA thin film. (d) Contact angle images and the calculated surface energy of as-deposited pEGDMA and pEGDMA exposed to water, respectively.

I–*V* characteristics were measured using an HP4156 semiconductor parameter analyzer. A custom-made bending mold was used to measure the *I*–*V* as a function of the bending radius, and the bending endurance also was evaluated by a custom-made bending machine. Secondary ion mass spectrometry (IMS7f) and XPS (Sigma Probe) were utilized to identify the components of the fabricated device. Specifically, FT-IR was used for the characterization of the pEGDMA before and after the polymerization process. An AFM (XE100) analysis was also conducted to assess the surface roughness of the coated polymer on various substrates. The filamentary conduction is analyzed by means of localized current mapping using a C-AFM (MultiMode 8). The preparation of a discission sample to observe the cross-sectional image of the i-RRAM was done using a focused ion beam (Helios Nanolab) after a protective coating of carbon and platinum in sequence was applied. The direct observation of the carbon filament was achieved by means of high-resolution TEM (JEM-ARM200F), after which EDS mapping (Quantax 400) was used to identify the components of each layer before and after the memory operation. Electron energy loss spectroscopy (Gatan Enfina) was used to extract the energy band gap of the pEGDMA. Then, ultraviolet photoelectron spectroscopy (VG Scientific, Sigma Thermo) was applied to detect the lowest unoccupied molecular orbital, which finally enabled the determining energy band structure of the pEGDMA *via* the calculation of the highest occupied molecular orbital. The test of the i-RRAM operation in water was conducted as follows. A minicontainer made of polydimethylsiloxane (PDMS) was prepared. The role of the minicontainer was to prevent an electrical short between each probing pad connected to the TE and the BE. In detail, Sylgard 184 (Sigma Aldrich) and a curing agent were mixed at a ratio of 10:1. Afterward, this was loaded into a vacuum chamber to remove bubbles. The PDMS mixture was sequentially coated onto a bare silicon wafer by spin coating, during which the silicon wafer serves only as a flat substrate. An annealing process was then applied at 110 °C for 15 min to solidify the PDMS. Thereafter, a hole with a diameter of 4 mm was formed using a manual puncher. The minicontainer was then ready. Finally, the stability of the pEGDMA against water was confirmed by tracing the invariance of the chemical bonding, surface morphology, and surface energy, which were evaluated using FT-IR, AFM, and the measurement of the contact angle, respectively.

Conflict of Interest: The authors declare no competing financial interest.

Acknowledgment. This work was supported by the Center for Integrated Smart Sensors funded by the Ministry of Science, ICT & Future Planning as Global Frontier Project (CISS-2011-0031848). This research was partially supported by the Pioneer Research Center Program through the National Research Foundation of Korea funded by the Ministry of Science, ICT & Future Planning (Grant 2012-0009594). This work was supported by Global Ph.D. Fellowship Program through the National Research Foundation of Korea (NRF) funded by the Ministry of Education (Grant No. 2014H1A2A1022137).

Supporting Information Available: The introduction of the iCVD process and the characterization of the applied polymer, a description of the strength of the iCVD process, the extracted data of the energy band structure of the polymer used as the resistive switching layer, an analysis of the fabricated device, a description of the features of the i-RRAM, and various analyses to verify the chemical stability of this polymer in water are provided. The Supporting Information is available free of charge on the ACS Publications website at DOI: 10.1021/acsnano.5b02199.

REFERENCES AND NOTES

1. Lee, S.; Kim, W.; Yong, K. Overcoming the Water Vulnerability of Electronic Devices: A Highly Water-Resistant ZnO Nanodevice with Multifunctionality. *Adv. Mater.* **2011**, *23*, 4398–4402.
2. Yang, Y.; Lu, W. Nanoscale Resistive Switching Devices: Mechanisms and Modeling. *Nanoscale* **2013**, *5*, 10076–10092.
3. Ling, Q.-D.; Liaw, D.-J.; Zhu, C.; Chan, D. S.-H.; Kang, E.-T.; Neoh, K.-G. Polymer Electronic Memories: Materials, Devices and Mechanisms. *Prog. Polym. Sci.* **2008**, *33*, 917–978.
4. Lin, W.-P.; Liu, S.-J.; Gong, T.; Zhao, Q.; Huang, W. Polymer-Based Resistive Memory Materials and Devices. *Adv. Mater.* **2014**, *26*, 570–606.
5. Lee, T.; Chen, Y. Organic Resistive Nonvolatile Memory Materials. *MRS Bull.* **2012**, *37*, 144–149.
6. Cho, B.; Song, S.; Ji, Y.; Kim, T.-W.; Lee, T. Organic Resistive Memory Devies: Performance Enhancement, Integration, and Advanced Architectures. *Adv. Funct. Mater.* **2011**, *21*, 2806–2829.
7. Sawa, A. Resistive Switching in Transition Metal Oxides. *Mater. Today* **2008**, *11*, 28–36.
8. Yague, J. L.; Coclite, A. M.; Petruczok, C.; Gleason, K. K. Chemical Vapor Deposition for Solvent-Free Polymerization at Surfaces. *Macromol. Chem. Phys.* **2013**, *214*, 302–312.
9. Im, S. G.; Gleason, K. K. Solvent-Free Modification of Surfaces with Polymers: The Case for Initiated and Oxidative Chemical Vapor Deposition (CVD). *AIChE J.* **2011**, *57*, 276–285.
10. Chu, C. W.; Ouyang, J.; Tseng, J.-H.; Yang, Y. Organic Donor-Acceptor Systems Exhibiting Electrical Bistability for Use in Memory Devices. *Adv. Mater.* **2005**, *17*, 1440–1443.
11. Lai, Y.-C.; Ohshimizu, K.; Lee, W.-Y.; Hsu, J.-C.; Higashihara, H.; Ueda, M.; Chen, W.-C. Electrically Bistable Memory Devices Based All-Conjugated Block Copolythiophenes and Their PCBM Composite Films. *J. Mater. Chem.* **2011**, *21*, 14502–14508.
12. Dearnaley, G.; Morgan, D. V.; Stoneham, A. M. A Model for Filament Growth and Switching in Amorphous Oxide Films. *J. Non-Cryst.* **1970**, *4*, 593–612.
13. Prime, D.; Paul, S. Overvies of Organic Memory Devices. *Philos. Trans. R. Soc. London, Ser. A* **2009**, *367*, 4141–4157.
14. Coclite, A. M.; Howden, R. M.; Borrelli, D. C.; Petruczok, C. D.; Yang, R.; Yague, J. L.; Ugur, A.; Chen, N.; Lee, S.; Jo, W. J.; *et al.* CVD Polymers: A New Paradigm for Surface Modification and Device Fabrication. *Adv. Mater.* **2013**, *25*, 5392–5423.
15. Moon, H.; Seong, H.; Shin, W. C.; Park, W.-T.; Kim, M.; Lee, S.; Bong, J. H.; Noh, Y.-Y.; Cho, B. J.; Yoo, S.; *et al.* Synthesis of Ultrathin Polymer Insulating Layers by Initiated Chemical Vapour Deposition for Low-Power Soft Electronics. *Nat. Mater.* **2015**, 10.1038/NMAT4237.
16. Lee, L. H.; Gleason, K. K. Cross-Linked Organic Sacrificial Material for Air Gap Formation by Initiated Chemical Vapor Deposition. *J. Electrochem. Soc.* **2008**, *155*, G78–G86.
17. Cho, B.; Yun, J.-M.; Song, S.; Ji, Y.; Kim, D.-Y.; Lee, T. Direct Observation of Ag Filamentary Pahts in Organic Resistive Memory Devices. *Adv. Funct. Mater.* **2011**, *21*, 3976–3981.
18. Yang, Y. C.; Pan, F.; Liu, Q.; Liu, M.; Zeng, F. Fully Room-Temperature-Fabricated Nonvolatile Resistive Memory for Ultrafast and High-Density Memory Application. *Nano Lett.* **2009**, *9*, 1636–1643.
19. Wang, Z.; Zeng, F.; Yang, J.; Chen, C.; Pan, F. Resistive Switching Induced by Metallic Filaments Formation through Poly(3,4-ethylene-dioxythiophene):Poly(styrenesulfonate). *ACS Appl. Mater. Interfaces* **2012**, *4*, 447–453.
20. Pender, L. F.; Fleming, R. J. Memory Switching in Glow Discharge Polymerized Thin Films. *Appl. Phys. Lett.* **1975**, *46*, 3426–3431.
21. Lampert, A.; Mark, P. *Current Injection in Solids*; Academic: New York, 1970.
22. Song, S.; Kim, T.-W.; Cho, B.; Ji, Y.; Lee, T. Nonvolatile Write-Once-Read-Many Times Memory Devices Based on the Composites of Poly(4-vinylphenol)/Vulcan XC-72. *J. Nanosci. Nanotechnol.* **2011**, *11*, 4492–4495.
23. Baek, S.; Lee, D.; Kim, J.; Hong, S.-H.; Kim, O.; Ree, M. Novel Digital Nonvolatile Memory Devices Based on Semiconducting Polymer Thin Films. *Adv. Funct. Mater.* **2007**, *17*, 2637–2644.
24. Gao, S.; Song, C.; Chen, C.; Zeng, F.; Pan, F. Dynamic Processes of Resistive Switching in Metallic Filament-Based Organic Memory Devices. *J. Phys. Chem. C* **2012**, *116*, 1795–17959.
25. Joo, W.-J.; Choi, T.-L.; Lee, K.-H.; Chung, Y. Study on Threshold Behavior of Operation Voltage in Metal Filament-Based Polymer Memory. *J. Phys. Chem. B* **2007**, *111*, 7756–7760.
26. Carchano, H.; Lacoste, R.; Segui, Y. Bistable Electrical Switching in Polymer Thin Films. *Appl. Phys. Lett.* **1971**, *19*, 414–416.
27. Segui, Y.; Carchano, H. Switching in Polystyrene Films: Transition from On to Off State. *Appl. Phys. Lett.* **1976**, *47*, 140–143.
28. Fu, D.; Xie, D.; Feng, T.; Zhang, C.; Niu, J.; Qian, H.; Liu, L. Unipolar Resistive Switching Properties of Diamondlike Carbon-Based RRAM Devices. *IEEE Electron. Device Lett.* **2011**, *32*, 803–805.
29. Hunag, J. Y.; Chen, S.; Ren, Z. F.; Chen, G.; Dresselhasus, M. S. Real-Time Observation of Tubule Formation from Amorphous Carbon Nanowires under High-Bias Joule Heating. *Nano Lett.* **2006**, *6*, 1699–1705.
30. Sebastin, A.; Pauza, A.; Rossel, C.; Shelby, A.; Rodriguez, A. F.; Pozidis, H.; Eleftheriou, E. Resistance Switching at the Nanometer Scale in Amorphous Carbon. *New J. Phys.* **2011**, *13*, 013020.